Chapter 10

Energy deposition and radiation to electronics

F. Cerutti[1*], *R. Garcia Alia*[1*], *G. Lerner*[1], *M. Sabaté Gilarte*[1, 2] *and A. Tsinganis*[1†]

[1]CERN, Accelerator & Technology Sector, Switzerland
[2]University of Seville, Spain
[†] ELI Beamlines, Czech Republic
[*]Corresponding authors

10 Energy deposition and radiation to electronics

10.1 Energy deposition

10.1.1 Characterization of the radiation source

Proton–proton inelastic collisions taking place inside the four LHC detectors generate a large number of secondary particles with an average multiplicity of approximately 120 per single proton–proton interaction with 7 TeV beams, but with very substantial fluctuations over different events. Moving away from the interaction point (IP), this multiform population evolves, even before touching the surrounding material, because of the decay of unstable particles (in particular neutral pions decaying into photon pairs). Figure 10-1 illustrates the composition of the debris at 5 mm from the point of a 14 TeV centre of mass collision, featuring a ∼30% increase in the number of particles, due to the aforementioned decays, and a clear prevalence of photons (almost 50%) and charged pions (∼35%).

Most of these particles are intercepted by the detector and its forward region shielding, releasing their energy within the experimental cavern. However, the most energetic particles, emitted at small angles with respect to the beam direction, travel farther inside the vacuum chamber and reach the accelerator elements, causing a significant impact on the magnets along the insertion regions (IRs), in particular the final focusing quadrupoles, their associated corrector units, and the separation dipoles. Figure 10-1 also shows the breakdown of the debris components going through the aperture of the Target Absorber Secondaries (TAS), a protection element installed at 20 m from the IP on each side of the high luminosity detectors (ATLAS in IR1 and CMS in IR5) and consisting of a 1.8 m long copper core, featuring in the HL era a circular aperture of 60 mm diameter.

Despite the fact that the number of particles per collision leaving the TAS aperture is more than one order of magnitude lower than the total number of debris particles, they carry about 80% of the total energy, implying that 40% of the released energy at the IP exits on each side of the experiments. At the nominal HL-LHC luminosity (5×10^{34} cm^{-2} s^{-1}), this represents about 3800 W per side that is inevitably impacting upon the LHC elements and consequently dissipated in the machine and in the nearby equipment (e.g. electronics, racks, etc.) and in the tunnel walls.

It is fundamental to study how these particles are lost in order to implement the necessary protections for shielding sensitive parts of the LHC machine. For this purpose, Monte Carlo simulations of particle interactions with matter play an essential role, relying on a detailed implementation of physics models and an accurate 3D description of the region of interest [1][2].

In addition to the luminosity debris, which dominates energy deposition in the vicinity of the collision points, regular and accidental beam losses represent other relevant sources of radiation. In particular, beam halo particles caught in the collimators (see Chapter 5) initiate hadronic and electromagnetic showers, mainly in the betatron and momentum cleaning IRs, but also from the tertiary collimators around the experiments. The same happens with injection and dumping protection devices (see Chapter 14). Moreover, secondary particle showers are also originated by beam interactions with the residual gas inside the vacuum chamber along the length of the accelerator, as well as with dust fragments falling into the beam path.

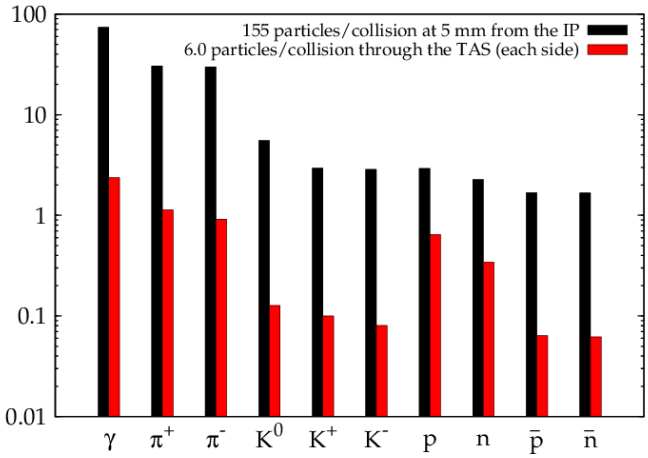

Figure 10-1: Breakdown of the debris particles per single proton–proton inelastic interaction at 5 mm from the interaction point (black) and at the exit of each 60 mm TAS aperture (red). Calculations have been carried out with FLUKA [3-8], as for all simulation results presented in this Chapter.

10.1.2 Triplet and separation dipole protection

As previously mentioned, the TAS absorber represents the interface between the detector and the accelerator on each side of the ATLAS and CMS caverns. On the other hand, its protection role is not needed for luminosities up to 0.2×10^{34} cm^{-2} s^{-1}, as in the LHCb insertion. In fact, the TAS effectiveness is limited to the first quadrupole, since its geometrical shadow gets soon spoiled by the effect of the magnetic field that bends a significant fraction of charged debris particles coming through its aperture, in particular high energy pions, against the quite larger quadrupole aperture. For this reason, the backbone element for the protection of the string of magnets up to the separation dipole (D1) is rather the beam screen equipped with dedicated tungsten alloy absorbers along its length. These absorbers are made of Inermet 180, which has a density of 18 g cm^{-3}, and reach their maximum thickness (of 16 mm in the first quadrupole Q1 and 6 mm elsewhere) at the magnet mid-planes, where the energy deposition is concentrated, as shown in 10-2.

In the latter, one can see that the beam screen structure is not in thermal contact with the magnet cold mass, allowing to evacuate its significant fraction of absorbed power at a different temperature. In fact, for an instantaneous luminosity of 5×10^{34} cm^{-2} s^{-1}, the total power collected by the 60 m long string of magnets amounts in the worst case (namely for vertical crossing) to more than 1200 W and is almost equally shared between the beam screen structure and the cold masses. For horizontal crossing, the total load is 6% less.

The combination between the focusing-defocusing field configuration and the crossing plane yields a characteristic longitudinal profile for the peak dose (and power density) in the superconducting coils, as reported in Figure 10-3 for the HL-LHCv1.3 optics with a 255 μrad half-angle and round beams at the IP.

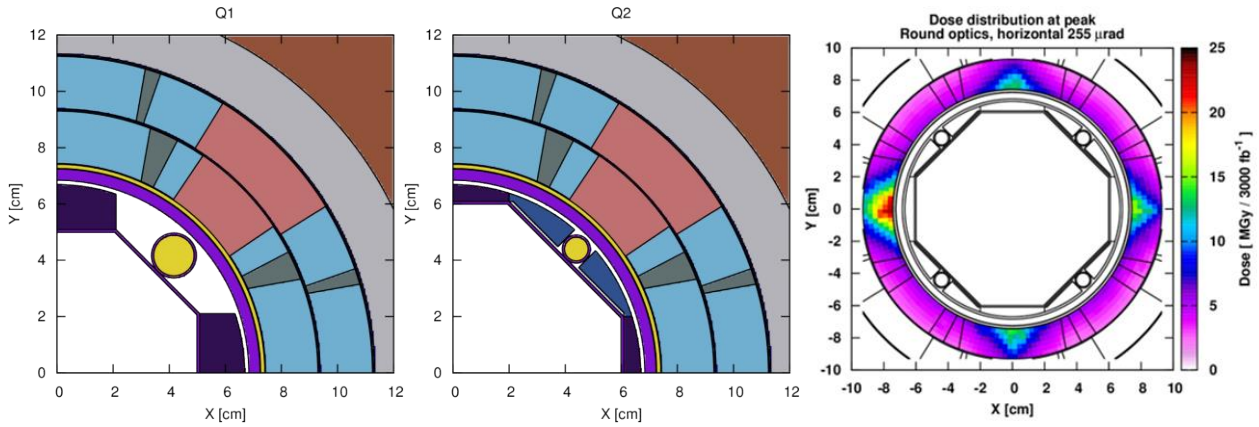

Figure 10-2: Cross-section of (a) the two modules of the first triplet quadrupole (Q1) and (b) all the other quadrupoles (Q2-Q3). The extension of the Inermet absorbers (dark blue) around the Helium (yellow) channel at 45°, implemented from Q2 onwards in alternation with pumping slot gaps, can be noted. The stainless steel cold bore is in violet, the Nb_3Sn coils are in light blue, the copper wedges are in dark grey, the titanium alloy poles are in red, the aluminium collar is in light grey, and the iron yoke is in brown. (c) Dose distribution in the coils at the IP end of the second Q2 module (Q2B) for horizontal crossing, representing the most exposed location.

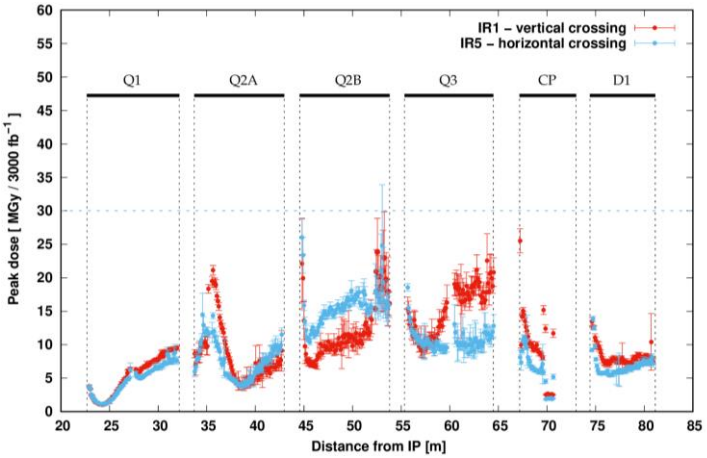

Figure 10-3: Peak dose profile in the superconducting coils of the single bore magnet string after 3000 fb^{-1}, for vertical (red) and horizontal (blue) crossing. The values are obtained by radially averaging over the innermost layer (≤ 3mm). Error bars indicate the statistical uncertainty. The discontinuity of the red points at the extremities of the orbit corrector dipoles in the CP and Q2A assembly is due to the fact that the inner coil layer, oriented to give a horizontal kick, intersects there the vertical plane. An analogous topological effect applies to the extremities of the superferric skew quadrupole at 70 m from the IP.

After the HL-LHC upgrade, the weakest point becomes the Q2B IP extremity for horizontal crossing, due to the effect of the preceding interconnect, where the amount of absorbing material is limited. A careful optimization of the interconnect design (see Figure 10-4), allowing for the extension of the Inermet absorbers as well as their installation in the embedded Beam Position Monitor (BPM), brought the maximum dose expectation down to 26 MGy for the nominal target of 3000 fb^{-1}, which is a level deemed to be sustainable by the coil insulator. However, the radiation resistance of the latter is challenged by the scaling to nearly 35 MGy for the ultimate goal of 4000 fb^{-1}, as indicated in Table 10-1.The target tolerances in the interconnect and BPM alignment do not affect the gain provided by this optimization. On the other hand, the maximum power density (radially averaged over the cable width) is predicted not to reach 3 mW/cm^3 at 5×10^{34} cm^{-2} s^{-1}, therefore

remaining below the Nb_3Sn (NbTi) quench limit of more than 60 mW/cm^3 (20-30 mW/cm^3) [9] with a considerable margin.

The coils of the three nested orbit correctors, located on different ends of the Q2A and Q2B cryostats and in the Corrector Package, are exposed to a lower dose if their inner layer is oriented in order to produce a vertical field, i.e. a horizontal kick, as assumed in Figure 10-3. It has to be noted that in such a configuration the inner layer crosses anyway the vertical plane at the magnet extremities, while remaining outside of it for most of the dipole length. In the case of the third corrector, this implies that for vertical crossing a dose of 25 MGy is locally reached on the IP side.

Table 10-1: Maximum dose (MGy) in the coils of the elements of the Q1–D1 string for the nominal and ultimate integrated luminosity targets.

Magnet	3 ab^{-1}	4 ab^{-1}	Magnet	3 ab^{-1}	4 ab^{-1}
Q1A	6.5	8.5	Q1B	9.5	13
Orbit Corrector	18.5	24.5	Q2A	21	28
Q2B	26	34.5	Orbit Corrector	< 25	< 33
Q3A	18.5	24.5	Q3B	22	29
Orbit Corrector	25.5	34	Superferric Correctors	12.5	16.5
D1	14	18.5			

Out of the nine superferric magnets of the Corrector Package, detailed dose distributions were calculated only for the skew quadrupole, whose maximum value of 12–13 MGy, found again at the magnet extremity where the coils traverse the vertical and horizontal planes, is not expected to be approached in the following short correctors.

Some margin to reduce the maximum accumulated dose, and so to increase the triplet lifetime, can be obtained if operating at minimal crossing angle with the envisaged levelling schemes, which yield a 10% improvement. Moreover, a transverse IP displacement in the crossing plane along the direction opposite to the beam transverse momentum, which is equivalent to a triplet displacement in the direction of the latter, has been found to have the potential for a further substantial gain, up to a 50% lifetime increase for a 2 mm displacement.

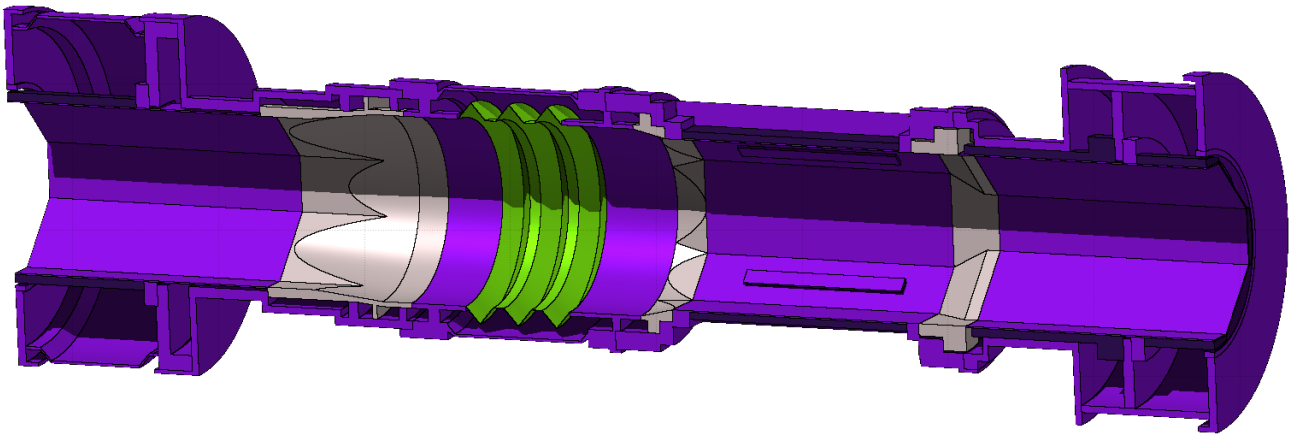

Figure 10-4: FLUKA model of the triplet interconnect, including an octagonal BPM.

10.1.3 Matching section protection

The transition from the single bore hosting the two counter-rotating beams to the two separate beam chambers (referred to as Y chamber) is embedded in the TAXN (Target Absorber Neutral, previously named simply TAN for the LHC layout), another massive absorber, with a 3.3 m long copper core, aimed at intercepting the neutral component of the collision debris, mostly photons and neutrons. The TAXN absorber provides a substantial protection to the double bore recombination dipole (D2) and the four main quadrupole assemblies of the matching section (see Figure 10-5), including dipole correctors.

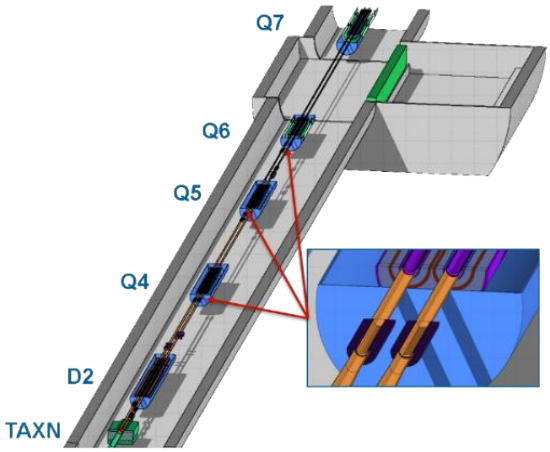

Figure 10-5: Geometry model of the future matching section layout. The frame zooms in on the additional TCLM masks.

However, the HL-LHC layout features a shorter D1–D2 distance, implying a lower beam separation in the TAXN, coupled to a very significant enlargement of its twin pipes, due to optics requirements. These design changes, together with an almost double-crossing angle and an important increase of the mechanical aperture of the upstream elements, lead to a weakening of the TAXN effectiveness. In fact, apart from the luminosity rise, the number of debris particles entering the matching section per primary collision is much larger than in the case of the current machine. This is illustrated in Figure 10-6, where the debris particle distribution at the exit of the TAXN outgoing beam pipe is shown for both the LHC and the HL-LHC. The number of protons is increased by about 30% (from 0.12 to 0.16 protons/collision), while the number of photons and neutrons is about seven times higher (from 0.06 to 0.41 particles/collision). Moreover, the beam size enlargement at this location implies that a collimator set at the same aperture in beam σ is less effective in intercepting debris particles, as clearly revealed in the figure by the number of particles left inside the beam envelope.

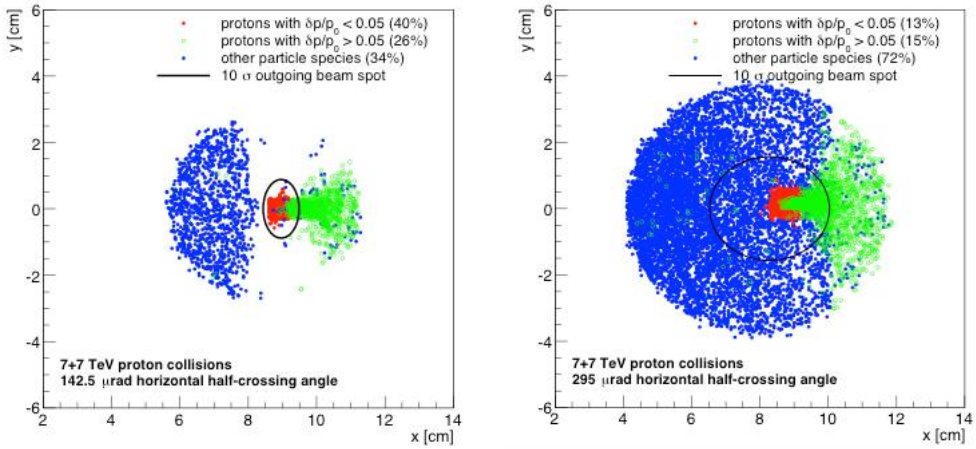

Figure 10-6: Debris particle distribution at the exit of the outgoing beam pipe of the TAXN, (left) for the LHC; (right) for the HL-LHC. Red points indicate protons with magnetic rigidity within 5% with respect to beam protons and green points indicate protons with lower magnetic rigidity. Blue points indicate neutral particles (photons and neutrons). The same number of collisions is simulated in both cases. The black ellipse shows the 10 σ outgoing beam envelope for round beam optics.

Therefore, the cold magnet shielding has to be strengthened, by complementing the TCL (Target Collimator Long) physics debris collimators on the outgoing beam with 1 m long tungsten alloy warm masks put in front of the cryostats and matching the aperture of the following beam screen, without altering the magnet design. Additionally, the first collimator, located between TAXN and D2, requires a special design with thicker jaws (TCLX4), in order to assure an adequate transverse coverage. The incoming beam pipe benefits from the

presence of the TCT (Target Collimator Tertiary) collimators that, while cleaning by design the incoming halo, also play a role in intercepting the debris propagating in the opposite direction. This scheme prevents the risk of debris induced quenches, keeping the power density in the coils below 1 mW/cm^3 for the reference luminosity of 5×10^{34} cm^{-2} s^{-1}, with the three TCL collimators set at 14 σ, equivalent to 21, 7 and 3 mm half gaps, respectively. Corresponding dose values after 3000 fb^{-1} are predicted to remain below 10 MGy, except for the D2, locally exceeding by 15% that limit as reported in Table 10-2. Nevertheless, the value locally reachable in the coils on the IP end of the Q4 cryostat, not closely preceded by a collimator, critically depends on the accuracy of the aperture and transverse alignment of the upstream mask, considering that a 2 mm discrepancy can lead it beyond 30 MGy.

Table 10-2: Maximum dose [MGy] in the coils of the elements of the D2 assembly for the nominal and ultimate integrated luminosity targets.

Magnet	3 ab^{-1}	4 ab^{-1}	Magnet	3 ab^{-1}	4 ab^{-1}
D2	11.5	15	Correctors	< 5	< 6

Figure 10-7 clearly shows that the leakage through the TAXN is minimized in case of vertical crossing, where the main spot in between the TAXN twin apertures is produced by neutral particles (photons and neutrons) hailing from the IP. Its vertical position reflects the crossing angle polarity. A further hot spot can be recognized on the lower edge of the outgoing beam bore (at positive x), due to protons far enough from the beam energy so that they are bent by the triplet quadrupoles on the side opposite to the crossing angle and then moved by the separation dipole in the external direction. For horizontal crossing, the neutral cone from the IP has instead a significantly larger overlap with the outgoing beam aperture, inducing in the D2, which is the most exposed magnet collecting of a total power amounting to 33 W, twice as much its load for vertical crossing.

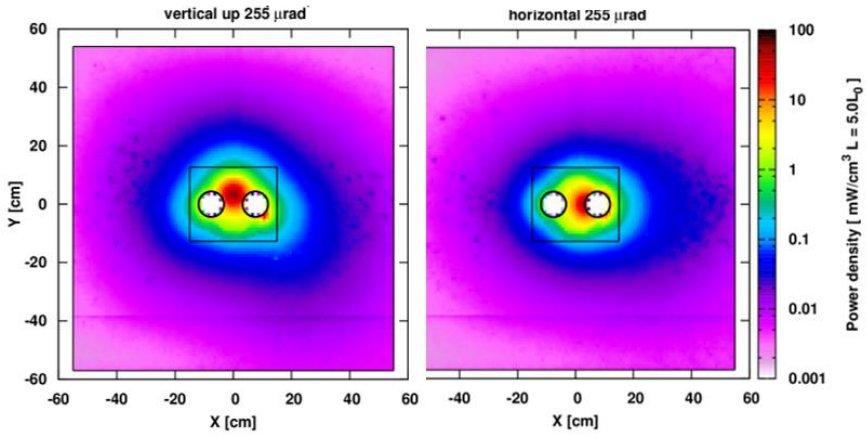

Figure 10-7: Absorbed power density distribution in the most impacted TAN slice, for vertical (left) and horizontal (right) beam crossing.

10.1.4 Dispersion suppressor protection

The most forward TCL collimator, in the straight section Half-Cell 6, provides a good cleaning of the initial part of the Dispersion Suppressor (DS), where the beam lines get bent through the LHC main dipoles and no layout modification is planned for the HL-LHC era. This is illustrated in Figure 10-8, where the progressive collimator closure translates into a substantial reduction in the number of debris particles impacting the beam screen. The tighter half gap considered in the figure is meant to indicate the cleaning sensitivity, but cannot be operationally adopted, since it would break the collimator hierarchy and, moreover, would excessively expose the metallic jaws to accidental events, such as an asynchronous beam dump. Anyway, beyond the TCL6 range, far losses are expected in the DS odd half-cells, according to the periodicity of the single turn dispersion, as regularly observed already in the LHC operation. In fact, they originate from protons subject to diffraction at

the IP, affected by a magnetic rigidity deficit of the order of 1% and therefore destined to touch the horizontal boundary of the mechanical aperture towards the centre of the ring.

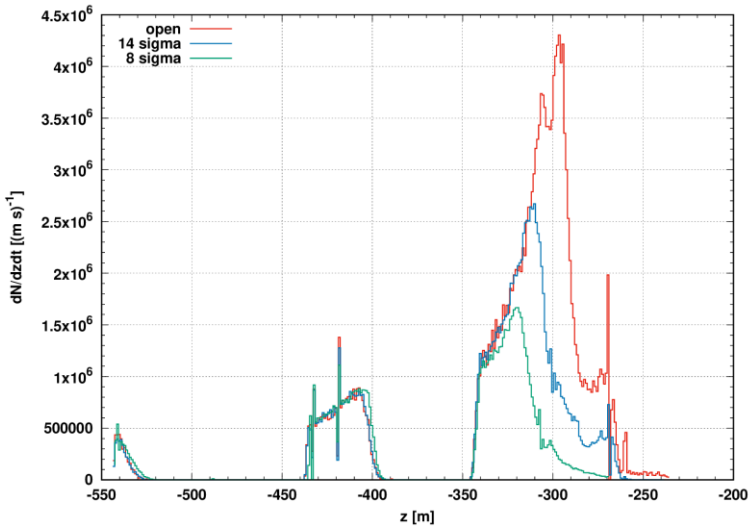

Figure 10-8: Loss maps in the DS for different TCL6 settings, normalized to the nominal instantaneous luminosity of 5×10^{34} cm^{-2} s^{-1}.

As a consequence, maximum doses at the level of 20 MGy are predicted to be accumulated in the superconducting coils of the Half-Cell 9 for a 3000 fb^{-1} integrated luminosity. On top of that, actual imperfections in the machine aperture may locally worsen the picture. Such values are deemed to be excessive for the dipole corrector in the Half-Cell 9 on the left of IP1 and IP5 (considering the layout asymmetry), due to its lower radiation resistance, and mitigation actions are being considered. Respective peak power densities appear less severe, being of the order of 1 mW/cm^3 for the reference instantaneous luminosity of 5×10^{34} cm^{-2} s^{-1}.

10.2 Radiation to electronics

10.2.1 Introduction

A specific problem is represented by the sensitivity of electronics to radiation. The above described particle debris emerging from the IP (together with the additional loss contribution from beam-gas interactions, which however is not expected to bring a significant increase) will impact equipment in the LHC tunnel and areas adjacent to it (UJs, RRs). Installed (present or future) electronic systems (e.g. controls, powering, protection…) are either fully commercial or based on commercial-off-the-shelf (COTS) components, both possibly affected by radiation. This includes the immediate risk of single event effects (SEE) and a possible direct impact on beam operation, as well as in the long-term cumulative dose effects (impacting the component/system lifetime) that additionally have to be considered.

For the tunnel equipment in the existing LHC, radiation was only partially, and relatively late, considered as a design criterion prior to construction. Most of the equipment placed in adjacent and partly shielded areas was neither conceived nor tested for their actual radiation environment. Therefore, given the large amount of electronics being installed in these areas, in 2008 a CERN-wide project called Radiation To Electronics (R2E) [10] was initiated to quantify the danger of radiation-induced failures and to mitigate the risk for beam operation to below one failure per week. The respective mitigation process, mainly through shielding and relocation, was based on a detailed analysis of the radiation fields involved, intensities and related Monte Carlo calculations; radiation monitoring and benchmarking; the behaviour of commercial equipment/systems and their use in the LHC radiation fields; as well as radiation tests with dedicated test areas and facilities [10][11].

In parallel, radiation-induced failures were analysed in detail in order to confirm early predictions of failure rates, as well as to study the effectiveness of implemented mitigation measures. Figure 10-9 shows the actual number of SEE failures measured during 2011 and 2012 operations, the achieved improvement (note that the failure rate measured during 2011 already benefitted from mitigation measures implemented during 2009 and 2010), as well as the goal for operation after LS1 and during the HL-LHC era. As can be seen in Table 10-3, the ~0.5 dumps/fb^{-1} objective was reached for the 2016-18 LHC operation period in Run 2, after the LS1 relocation, shielding and upgrade activities.

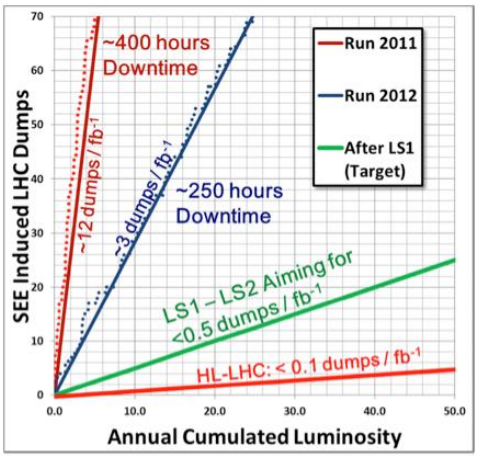

Figure 10-9: LHC beam dumps due to single event effects against beam luminosity. Dots (2011 and 2012) refer to measurements, whereas lines show annual averages for both past and future operations.

Aiming for annual luminosities of 250 fb^{-1}, it is clear that machine availability has to be maximized during the HL-LHC period in order to successfully achieve the physics goal. This implies that existing electronics systems are either installed in fully safe areas, sufficiently protected by shielding, or are made adequately radiation tolerant.

Table 10-3: Number of R2E suspected dumps during Run 2 operation.

Year	R2E dumps				Integrated Luminosity (fb^{-1})	R2E dumps per fb^{-1}
	QPS	EPC	Other	Total		
2015	2	5	-	7	4.2	1.7
2016	0	6	-	6	40	0.15
2017	1	10	-	11	50	0.22
2018	14	11	3	28	60	0.46

The last statement implies that existing equipment, as well as any future equipment that may be installed in R2E critical areas, must be conceived in a specific way.

Radiation damage to electronics is often considered in satellite and human space flight and was also to different degrees of detail regarded in the LHC experiment electronics design and qualification. However, it is important to note that the radiation environment encountered at the LHC accelerator, the high number of electronics systems and components partly exposed to radiation, as well as the actual impact of radiation-induced failures, differ strongly from the context of satellite and human space flight applications. While design, test, and monitoring standards are already well defined for the latter, additional constraints, but in some cases also simplifications – mainly related to the ability of upgrading equipment and improving the related radiation tolerance at regular intervals - have to be considered for the accelerator environment.

The mixed particle type and energy field encountered in the relevant LHC areas is composed of charged and neutral hadrons (protons, pions, kaons, and neutrons), photons, electrons, and muons ranging from thermal energies up to the GeV range. This complex field has been extensively simulated by the FLUKA Monte Carlo code and benchmarked in detail for radiation damage issues at the LHC [12][13]. As discussed above, the observed radiation is due to particles generated by proton–proton (or ion–ion) collisions in the LHC

experimental areas, distributed beam losses (protons, ions) around the machine, and to beam interaction with the residual gas inside the beam pipe. The proportion of the different particle species in the field depends on the distance and angle with respect to the original loss point, as well as on the amount (if any) of installed shielding material. In this environment, electronics components and systems exposed to a mixed radiation field will experience three different types of radiation damage: displacement damage, damage from the total ionizing dose (TID), and Single Event Effects (SEEs). The latter range from single event or multiple bit upsets (SEUs or MBUs), transients (SETs) up to possible destructive latch-ups (SELs), destructive gate ruptures, or burn-outs (SEGRs and SEBs).

The first two groups are of cumulative nature and are measured through TID and non-ionizing energy deposition (non-ionizing energy losses (NIEL), generally quantified through accumulated 1 MeV neutron equivalent fluence), where the steady accumulation of defects causes measurable effects that can ultimately lead to device failure. As for stochastic SEE failures, they form an entirely different group, since they are due to ionization by a single particle and are able to deposit sufficient energy to perturb the operation of the device. They are characterized in terms of their probability of occurring as a function of accumulated high energy (> 20 MeV) hadron (HEH) fluence, incorporating also the weighted contribution of lower energy neutrons [14]. The probability of failure will strongly depend on the device as well as on the flux and nature of the particles.

10.2.2 Radiation environment and effects during Run 2

During Run 1 and Run 2 LHC operation, the radiation levels in the LHC tunnel and in the (partly) shielded areas have been extensively measured using the CERN RadMON system [15], which is dedicated to the analysis of radiation levels possibly impacting installed electronics equipment. In combination with other radiation monitors (e.g. Beam Loss Monitors, optical fibres) and FLUKA calculations, the radiation levels in the machine can be accurately measured and linked with the operational parameters of the machine.

Table 10-4 summarizes the level of accumulated HEH fluence measured during the Run 2 nominal operation years for the most critical LHC areas where electronics equipment is installed and that are relevant for the HL-LHC project. The HEH fluence measurements are based on the RadMON reading of the SEUs of SRAM memories whose sensitivity has been extensively calibrated in various facilities. In the case of LHC tunnel locations, RadMONs are typically placed below the interconnects (at 70 cm from the floor level) and are therefore slightly more exposed than the electronic racks themselves, which are located below the magnets.

Moreover, in the RE alcoves, which are shielded galleries next to the LHC ARCs, the measured levels by the RadMONs on the tunnel side of the alcoves are, as expected, compatible with those of the arc RadMONs in the tunnel itself. Inside the alcove, the vast majority of RadMONs measure no SEU events at all, setting an upper limit to the annual fluence of 10^6 HEH/cm^2/yr. Therefore, in practical terms such values are compatible with surface level cosmic neutron flux.

It is worth noting that the changes during Run 2 in the annual radiation levels of the RRs and Cells 8/9 of the Dispersion Suppressor in IP1 and IP5 are mainly related to the different Roman Pot and TCL6 configurations. For the HL-LHC, the situation will be that all TCL debris collimators (4, 5 and 6) will be in closed position (14σ) therefore protecting Half-Cell 8 (and partially 9) in the DS at the expense of generating large radiation levels in the RRs. It is worth noting that during 2018, operation with the TCL6 open reduced the radiation levels in the IP1 and IP5 RRs, but increased them in Half-Cell 8 and beginning of Half-Cell 9 of the DS, leading to an overall increase in the R2E events per unit integrated luminosity, as reflected in Table 10-3.

Likewise, the 2018 increase in the annual radiation levels in IP7 (both RR and DS) is related to the increase of a factor ~3 of protons lost in the primary collimation system in 2018 with respect to 2016 and 2017 due to the reduced dynamic aperture linked to the crossing angle and beta-star reduction.

Table 10-4: HEH levels in different LHC locations critical for electronics operation as measured during Run 2 with the RadMON system.

LHC area	Zone Type	2016 (HEH/cm^2)	2017 (HEH/cm^2)	2018 (HEH/cm^2)
UJ14/161	Shielded	8.3×10^8	8.9×10^8	2.7×10^8
RR13/17	Shielded	5.4×10^7	3.9×10^8	1.6×10^8
UJ56	Shielded	6.7×10^8	8.1×10^8	8.5×10^8
RR53/57	Shielded	1.9×10^8	5.1×10^8	3.9×10^8
UJ76	Shielded	3.4×10^7	7.9×10^7	1.7×10^8
RR73/77	Shielded	1.6×10^7	1.8×10^7	6.6×10^7
UX85	Shielded	5.3×10^8	4.7×10^8	6.0×10^8
US85	Shielded	1.4×10^8	1.2×10^8	1.4×10^8
IP1 Half-Cell 8	Tunnel (DS)	9.9×10^8	8.5×10^8	1.7×10^{11}
IP5 Half-Cell 8	Tunnel (DS)	3.2×10^8	4.9×10^8	1.3×10^{11}
IP1 Half-Cell 9	Tunnel (DS)	3.7×10^{10}	1.0×10^{10}	2.9×10^{10}
IP5 Half-Cell 9	Tunnel (DS)	4.1×10^{10}	3.4×10^{10}	5.2×10^{10}
IP7 Half-Cell 9	Tunnel (DS)	7.3×10^8	2.1×10^8	7.3×10^8
IP1 Half-Cell 11	Tunnel (DS)	6.0×10^{10}	7.8×10^{10}	4.5×10^{10}
IP5 Half-Cell 11	Tunnel (DS)	3.4×10^{10}	5.1×10^{10}	5.2×10^{10}
Rest of DS and ARC	Tunnel	$\sim 5 \times 10^7$		

10.2.3 FLUKA R2E simulations for IP1 and IP5

In combination with projections based on presently measured radiation levels and expected future scaling, FLUKA simulations are an essential tool in defining radiation levels for future operation, especially for cases involving new layouts and/or beam optics scenarios.

Dedicated maps of R2E relevant quantities in the tunnel and adjacent areas of the high luminosity experimental insertions (IP1 and IP5), in their HL-LHC configuration, are available through FLUKA simulations. A first study focused on the energy deposition and R2E relevant levels in the inner triplet and matching section, extending up to 260m from the IPs, up to Half-Cell 7 [16]. In this area, the radiation levels in the HL-LHC tunnel at locations relevant for the equipment (i.e. 1.6m from the beam line) and for the full operational period (3000 fb^{-1}) will be mostly above 10 kGy and 10^{13} n_{eq}/cm^2, reaching maximum values of over an order of magnitude larger. Therefore, such values clearly exclude the use of accelerator systems based on commercial electronic components, and dedicated Application Specific Integrated Circuits (ASIC) and other radiation hardened by design components would need to be developed for such applications.

A case of special interest in this region are the radiation levels immediately downstream D1, a suitable location for the cold bypass diodes protecting the inner triplet magnet circuit. Provided the electrical parameters of such high-current diodes are expected to degrade with radiation, thus potentially compromising the integrity of the machine, a dedicated radiation level study was carried out to define the radiation hardness targets for the diode. The main results of such study are shown in Figure 10-10, reflecting that a potentially adequate location for the diode from a radiation environment perspective would be around 83m from the IP. At this location, the

[1] The apparent reduction in the HEH hadron levels in 2018 in UJ14/16 is attributed to the direct measurement of the R-factor (contribution of thermal neutrons to the total SEU rate) which, as not measurable in previous years, was assumed as a worst-case value in terms of respective HEH flux.

neutron equivalent fluence (main contributor of the diode degradation) is at a stable minimum of ~2×10^{14} n/cm^2, and the ionizing dose is below 50 kGy, before abruptly increasing due to the absence of the shielding provided by the D1 magnet structure.

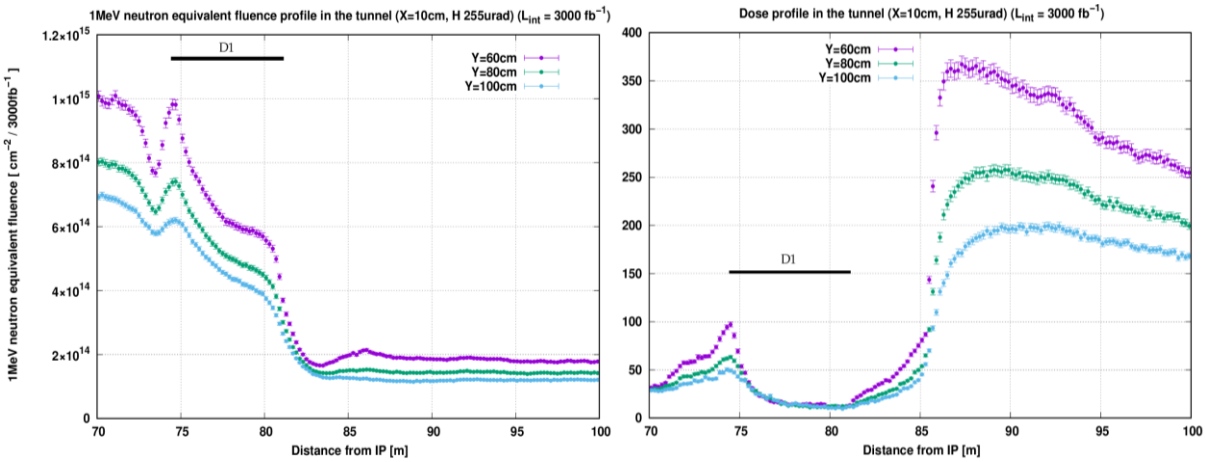

Figure 10-10: Simulated radiation levels in terms of 1-MeV neutron equivalent (left) and TID (right) for 3000 fb^{-1} HL-LHC operation near D1, at beam level in the horizontal direction perpendicular to the beam (X=0) and at different vertical positions (Y=60, 80 and 100 cm) for horizontal, IP5 crossing.

Owing to the harsh radiation environment in the LHC inner triplet and matching section, electronic systems for the machine elements installed in this area (e.g. inner triplet magnets) are hosted in the shielded alcoves. The latter are known as UJ (Junction Chamber) and UL (Liaison Gallery between Underground Works) in the case of the heavily shielded areas near the IPs; and as RRs for the lightly shielded areas roughly 240–260 m away from the IP. According to the dedicated FLUKA simulations, taking into account the detailed layout and beam optics aspects of the HL-LHC, the expected radiation levels in the shielded areas around IP1 and IP5 are summarized in Table 10-5.

Table 10-5: Expected annual radiation levels in IP1/IP5 shielded alcoves for the HL-LHC operation. Further details of the HL-LHC radiation environment are provided in Ref. [17].

Location	**HEH fluence (HEH/cm^2/yr)**	**TID (Gy)**	**1-MeV neutron equivalent fluence (cm^{-2})**
UJ14/16/56	3×10^9	6	5×10^{10}
UL14/16	1.2×10^8	< 1	$< 10^{10}$
RR13/17	1.4×10^{10}	25	7×10^{10}

An important implication of such levels is that equipment installed in the UJ and RR shielded areas will not only need to be tolerant to SEEs, but also qualified for cumulative TID and DD degradation, as the specified radiation levels for the HL-LHC are of a magnitude that implies potential lifetime issues for commercial parts. For the LHC, only the electronics installed in the tunnel was concerned about cumulative damage, the shielded electronics being mainly designed and qualified against SEEs.

Moving further away from the IP, as of Half-Cell 8 included, the LHC tunnel starts to host electronic racks for a broad variety of equipment (power converters, quench protection system, vacuum, cryogenics, beam instrumentation…). As shown in Section 10.1.2 related to the Run 2 operation, the Dispersion Suppressors of IP1 and IP5 are amongst the most hostile radiation areas with active commercial electronics in operation. Despite the robust radiation design of many of these systems, the 2018 experience in particular has shown that both SEE and lifetime radiation effects in this area of the machine can have a strong impact on the availability of the different systems and in turn that of the accelerator as a whole.

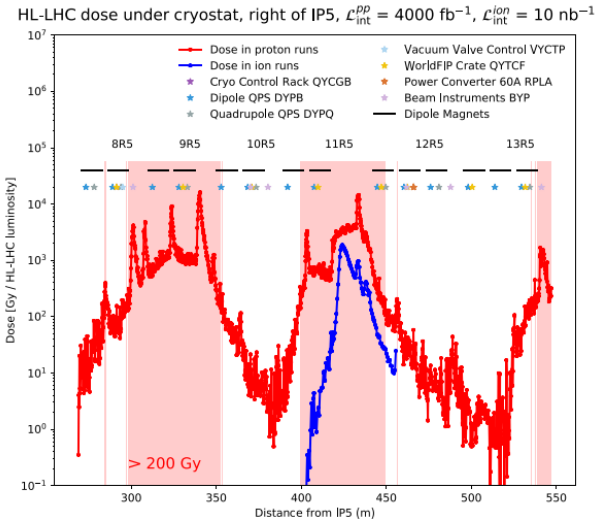

Figure 10-11: Simulated TID distribution for the equipment rack locations (70 cm below the beam) for both proton (4000 fb^{-1}) and ion (10 nb^{-1}) HL-LHC operation in IP1/5.

This will be even more the case for the HL-LHC, where losses in the DS, in fist approximation, are expected to increase with the integrated luminosity. The results of the dedicated FLUKA studies for this area of the machine, taking the protons lost on the beam screen from a first step simulation starting from the collisions in the IP, and propagating them and their produced showers in a second step, are shown in Figure 10-11. The radiation levels (e.g. dose) are scored below the magnets, at the location of the electronic racks, and both for proton and ion operation. As can be seen, whereas the ion losses, deriving from Bound Free Pair Production processes in the IP, are mainly located in the interconnect cryostat, losses during proton operation will affect very large portions of Half-Cells 9 and 11 hosting racks. Therefore, electronic designs for the latter will either need to be more robust than the present LHC tunnel qualification limit of 200 Gy, or racks will require relocation, often implying a significant cost, especially in terms of cabling.

10.2.4 Radiation hardness assurance implications

The radiation levels near IP1 and IP5 (Dispersion Suppressor and shielded areas), as well as elsewhere in the machine (not directly covered in this report, but described as radiation level specifications in Ref. [17]) pose a serious threat and constraint to the operation of electronics for critical HL-LHC systems. As a complementary activity to Work Package 10 in the HL-LHC, who is responsible for the definition of the expected radiation levels and validation of the related Radiation Hardness Assurance of the equipment; the Radiation to Electronics (R2E) project at CERN provides, in parallel to the HL-LHC, the necessary support for the actual electronic component selection and circuit architecture definition, as well as for the radiation qualification, both at component and system level.

The selection and qualification of the critical parts for a radiation tolerant system needs to be performed at a very early stage of the project, as the outcome of the radiation tests on the component can have a decisive impact on the system design. Radiation testing at component level is typically carried out using 200 MeV proton beams at the Paul Scherrer Institute (PSI), as well as in the CHARM mixed-field facility, both covering all three effects of radiation: TID, displacement damage and Single Event Effects. The cumulative radiation level targets will depend on the specific applications, but for parts of possible use across multiple HL-LHC systems, 1 kGy and 10^{13} n_{eq}/cm^2 are typically applied. For pure TID tests, the cobalt-60 facility at CERN provides a highly accessible and practical option. As for SEE testing, the upper limit to the acceptable cross-section will depend on the criticality of the part and the system, however values as low as ~10^{-13} cm^2/device may be required (as was the case e.g. for the analog-to-digital converter of the FGClite power converter controls system).

According to the expected HL-LHC radiation levels and availability objectives, the following Radiation Hardness Assurance (RHA) considerations apply:

- Radiation levels in the tunnel, especially in the DS areas exposed to high losses, will reach the HL-LHC lifetime values of ~1 kGy, therefore considerably exceeding the expected radiation lifetime of equipment presently installed in the machine, and posing a critical constraint to the selection of the system's architecture and selection of commercial components;
- Radiation levels in the UJ and RR shielded areas (~50–100 Gy for the full HL-LHC operation) will not only involve a threat in terms of Single Event Effects, but also related to commercial component lifetime.

Owing to the challenging radiation level and system availability requirements, as well as the very broad range and quantity of electronic components and systems installed in radiation areas, the component level radiation testing described above needs to be complemented with system level testing. The latter is performed in the CHARM facility at the PS East Area experimental complex, providing a unique opportunity of irradiating full-scale accelerator systems in representative functional and radiation conditions, and constituting the final RHA validation step before being approved for installation in radiation areas.

10.3 References

[1] N.V. Mokhov and I.L. Rakhno, Mitigating radiation loads in Nb_3Sn quadrupoles for the CERN Large Hadron Collider upgrades, *Phys. Rev. ST Accel. Beams* **9** (2006), DOI: 10.1103/PhysRevSTAB.9.101001.

[2] L.S. Esposito, F. Cerutti and E. Todesco, Fluka Energy Deposition Studies for the HL LHC, Conf. Proc. C130512, 2013, pp.TUPFI021.

[3] G. Battistoni *et al.*, Overview of the FLUKA code, Annals of Nuclear Energy 82 (2015), DOI: 10.1016/j.anucene.2014.11.007.

[4] T.T. Bohlen *et al.*, The FLUKA Code: Developments and Challenges for High Energy and Medical Applications, Nuclear Data Sheets 120, 211-214, 2014, DOI: 10.1016/j.nds.2014.07.049.

[5] V. Vlachoudis, FLAIR: A powerful but user friendly graphical interface for FLUKA, Proc. Int. Conf. Mathematics, Computational Methods & Reactor Physics, Saratoga Springs, New York, 2009, on CD-ROM, American Nuclear Society, LaGrange Park, IL, 2009, ISBN: 978-0-89448-069-0.

[6] A. Mereghetti *et al.*, The FLUKA LineBuilder and Element DataBase: Tools for Building Complex Models of Accelerator Beam Lines, IPAC2012, Conf. Proc. C1205201, 2012, pp.WEPPD071.

[7] S. Roesler, R. Engel and J. Ranft, The Monte Carlo event generator DPMJET-III, Proc. Monte Carlo 2000 Conference, Lisbon, October 23-26 2000, A. Kling, F. Barao, M. Nakagawa, L. Tavora, P. Vaz eds., Springer-Verlag Berlin, pp. 1033-1038, 2001, DOI: 10.1007/978-3-642-18211-2_166.

[8] A. Fedynitch, Cascade equations and hadronic interactions at very high energies, PhD Thesis, CERN-THESIS-2015-371.

[9] P.P. Granieri and R. van Weelderen, Deduction of Steady-State Cable Quench Limits for Various Electrical Insulation Schemes With Application to LHC and HL-LHC Magnets, *IEEE Transactions on Applied Superconductivity* **24**, (2014) 4802806, DOI: 10.1109/TASC.2014.2299797.

[10] R2E website. www.cern.ch/r2e.

[11] M. Brugger *et al.*, R2E Experience and outlook for 2012, Proc. LHC Performance workshop, Chamonix 2012, pp 13-18.

[12] K. Roed *et al.*, FLUKA simulations for SEE studies of critical LHC underground areas, *IEEE Trans. Nucl. Sci.* **58**, (2011) 932, DOI: 10.1109/TNS.2010.2097605.

[13] M. Battistoni *et al.*, FLUKA capabilities and CERN applications for the study of radiation damage to electronics at high-energy hadron accelerators, *Prog. Nucl. Sci. Tech.*, 2010, PNST10184-R1.

[14] K. Roed *et al.*, Method for Measuring Mixed Field Radiation Levels Relevant for SEEs at the LHC, *IEEE Trans. Nucl. Sci*. **59**, 2012, 1040, DOI: 10.1109/TNS.2012.2183677.

[15] G. Spiezia *et al.*, A New RadMon Version for the LHC and its Injection Lines, *IEEE Trans. Nucl. Sci*. **61**, (2014) 3424, DOI: 10.1109/TNS.2014.2365046.

[16] R. García Alía *et al*., "LHC and HL-LHC: Present and Future Radiation Environment in the High-Luminosity Collision Points and RHA Implications," in IEEE Transactions on Nuclear Science, vol. 65, no. 1, pp. 448-456, Jan. 2018, DOI: 10.1109/TNS.2017.2776107.

[17] G. Lerner *et al*., "HL-LHC Radiation level specification document", EDMS: 2302154.